# A Multi-Frequency Multi-Resolution Approach for GPR Microwave Imaging of Buried Objects

M. Salucci, L. Poli, and A. Massa

**Abstract**

This work presents a numerical validation of an innovative inverse scattering (*IS*) technique for the microwave imaging of buried objects through the deterministic inversion of wideband ground penetrating radar (*GPR*) data. The developed methodology is based on an iterative multi-focusing strategy and on a multi-frequency (*MF*) formulation of the *IS* equations. The minimization of the arising *MF* cost function is performed by a customized conjugate gradient (*CG*)-based solver. Some numerical results are presented in order to validate the effectiveness of the developed methodology under different operating conditions, by considering a variation of the shape/material of the unknown objects, as well as a variation of the level of noise on the measured time-domain total field. Moreover, a comparison with respect to a state-of-the-art approach based on a Frequency Hopping (*FH*) strategy is given, as well.

# 1 Definitions

## 1.1 Glossary

- $D_{inv}$: investigation domain;
- $D_{obs}$: observation domain;
- $N$: number of discretization cells in $D_{ind}$;
- $V$: number of views;
- $M$: number of measurement points;
- $F$: number of frequencies considered for the inversion;
- $(x_v, y_v)$: coordinates of the $v$-th source ($v = 1, \ldots, V$).
- $(x_m^v, y_m^v)$: coordinates of the $m$-th measurement point for the $v$-th view $v$, ($m = 1, \ldots, M$);
- $\varepsilon_{ra} = \frac{\varepsilon_a}{\varepsilon_0}$: relative electric permittivity for the upper half-space ($y > 0$);
- $\sigma_a$: conductivity for the upper half-space ($y > 0$);
- $\varepsilon_{rb} = \frac{\varepsilon_b}{\varepsilon_0}$: background relative electric permittivity;
- $\sigma_b$: background conductivity;

# 2 $MF-IMSA-CG$ vs. $FH-IMSA-CG$ - Performances vs. Noise

## 2.1 Square-shaped object ($\varepsilon_{r,obj}=5.0$, $\sigma_{obj}=10^{-3}$ [S/m])

### 2.1.1 Parameters

**Background**

Inhomogeneous and nonmagnetic background composed by two half spaces

- Upper half space ($y>0$ - air): $\varepsilon_{ra}=1.0$, $\sigma_a=0.0$;
- Lower half space ($y<0$ - soil): $\varepsilon_{rb}=4.0$, $\sigma_b=10^{-3}$[S/m];

**Investigation domain** ($D_{inv}$)

- Side: $L_{D_{inv}}=0.8$ [m];
- Barycenter: $\left(x_{bar}^{D_{inv}}, y_{bar}^{D_{inv}}\right)=(0.00,-0.4)$ [m];

**Time-Domain forward solver** ($FDTD$ - $GPRMax2D$)

- Side of the simulated domain: $L=6$ [m];
- Number of cells: $N^{FDTD}=750\times750=5.625\times10^5$;
- Side of the $FDTD$ cells $l^{FDTD}=0.008$ [m];
- Simulation time window: $T^{FDTD}=20\times10^{-9}$ [sec];
- Time step: $\Delta t^{FDTD}=1.89\times10^{-11}$ [sec];
- Number of time samples: $N_t^{FDTD}=1060$;
- Boundary conditions: perfectly matched layer ($PML$);
- Source type: Gaussian mono-cycle (first Gaussian pulse derivative, called "Ricker" in $GPRMax2D$)
  - Central frequency: $f_0=300$ [MHz];
  - Source amplitude: $A=1.0$ [A];

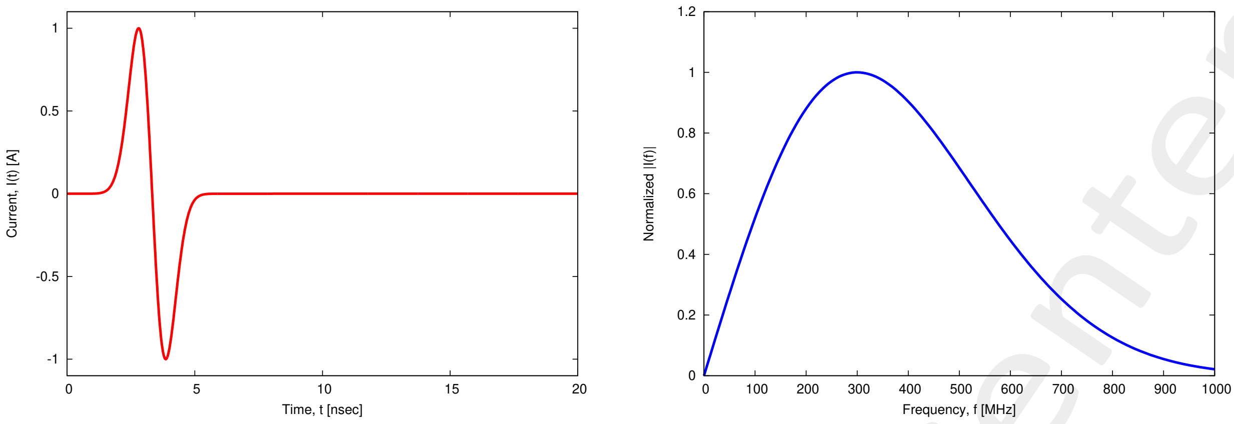


(a) (b)

Figure 1: *GPRMax2D* excitation signal. $(a)$ Time pulse, $(b)$ normalized frequency spectrum.

**Frequency parameters**

- Frequency range: $f \in [f_{min}, f_{max}] = [200.0, 600.0]$ [MHz] [?] ($-3$ [dB] bandwidth of the Gaussian Monocycle excitation centered at $f_0 = 300$ [MHz]);
- Frequency step: $\Delta f = 100$ [MHz] ($F = 5$ frequency steps in $[f_{min}, f_{max}]$);

| $f$ [MHz] | $\lambda_a$ [m] | $\lambda_b$ [m] | $f^*$ [MHz] |
|---|---|---|---|
| 200.0 | 1.50 | 0.75 | 200.5 |
| 300.0 | 1.00 | 0.50 | 297.6 |
| 400.0 | 0.75 | 0.37 | 401.1 |
| 500.0 | 0.60 | 0.30 | 498.1 |
| 600.0 | 0.50 | 0.25 | 601.6 |

Table 1: Considered frequencies and corresponding wavelength in the upper medium ($\lambda_a$, free space) and in the lower medium ($\lambda_b$, soil). $f^*$ is the nearest frequency sample available from transformed time-domain data, and represents the real frequency considered by the inversion algorithm.

**Scatterer**

- Type: square-shaped;
- Barycenter: $(x_{obj}, y_{obj}) = (-0.08, -0.24)$ [m];
- Side: $L_{obj,x} = L_{obj,y} = 0.16$ [m];
- Electromagnetic properties: $\varepsilon_{r,obj} = 5.0$, $\sigma_{obj} = 10^{-3}$ [S/m] ($\sigma_{obj} = \sigma_b$);
- Contrast function: $\tau = 1.0 + j0.0$

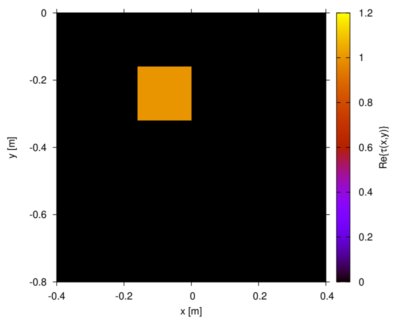


Figure 2: Actual object: offset square cylinder $\tau = 1.0$.

**Measurement setup**

- Considered frequency: $f_{min} = 200$ [MHz], $\lambda_b = 0.75$ [m].
- $\#DoFs = 2ka = \frac{2\pi}{\lambda_b} L\sqrt{2} = \frac{2\pi}{0.75} 0.8\sqrt{2} \simeq 9.5$;
- Number of views (sources): $V = 10$;
  - $\min\{x_v\} = -0.5$ [m], $\max\{x_v\} = 0.5$ [m];
  - height: $y_v = 0.1$ [m], $\forall v = 1, \dots, V$;
- Number of measurement points: $M = 9$;
  - $\min\{x_m\} = -0.5$ [m], $\max\{x_m\} = 0.5$ [m];
  - height: $y_m = 0.1$ [m], $\forall m = 1, \dots, M$;

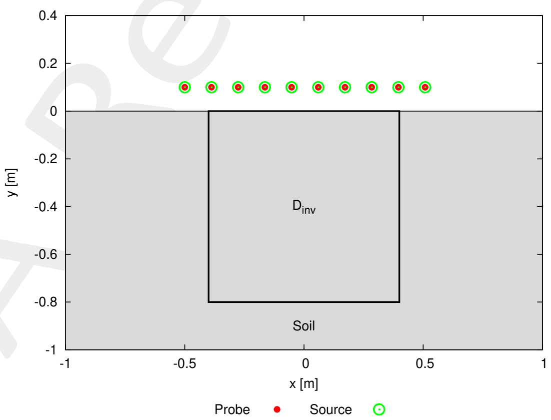


Figure 3: Location of the measurement points ($M = 9$) and of the sources ($V = 10$). Only one source is active for each view.

**Inverse solver parameters**

- **Shared parameters**
  - Weight of the state term of the functional: 1.0;
  - Weight of the data term of the functional: 1.0;

- Convergence threshold: $10^{-10}$;
- Variable ranges:
    * $\varepsilon_r \in [4.0, 5.2]$, $\sigma \in \left[8.0 \times 10^{-4}, 1.2 \times 10^{-3}\right]$ [S/m];
    * $\Re\left\{E_{tot}^{int}\right\} \in [-8, 8]$, $\Im\left\{E_{tot}^{int}\right\} \in [-8, 8]$;
- Degrees of freedom:
    * Considered frequency: $f_{min} = 200$ [MHz], $\lambda_b = 0.75$ [m];
    * $\frac{(2ka)^2}{2} = \frac{\left(2 \times \frac{2\pi}{\lambda_b} \times \frac{L\sqrt{2}}{2}\right)^2}{2} = 4\pi^2 \left(\frac{L}{\lambda_b}\right)^2 = 4\pi^2 \left(\frac{0.8}{0.75}\right)^2 \simeq 44.87$;
- Number of cells: $N = 49 = 7 \times 7$;
- Maximum number of $IMSA$ steps: $S = 4$;
- Side ratio threshold: $\eta_{th} = 0.2$;

- $MF - IMSA - CG$ **parameters**
    - Maximum number of iterations: $I = 200$;
- $FH - IMSA - CG$ **parameters**
    - Maximum number of iterations: $I = 400$;

**Signal to noise ratio (on $E_{tot}(t)$)**

- $SNR = \{50, 40, 30, 20\}$ [dB] + Noiseless data.

| SNR on $E_{tot}(t)$ [dB] | Av. SNR on $E_{scatt}(f)$ [dB] |
|---|---|
| 50 | 35 |
| 40 | 25 |
| 30 | 15 |
| 20 | 5 |

Table 2: Average $SNR$ measured on the scattered field in frequency domain.

### 2.1.2 Results

**Final reconstructions (@$f_{max} = 600$ [MHz])**

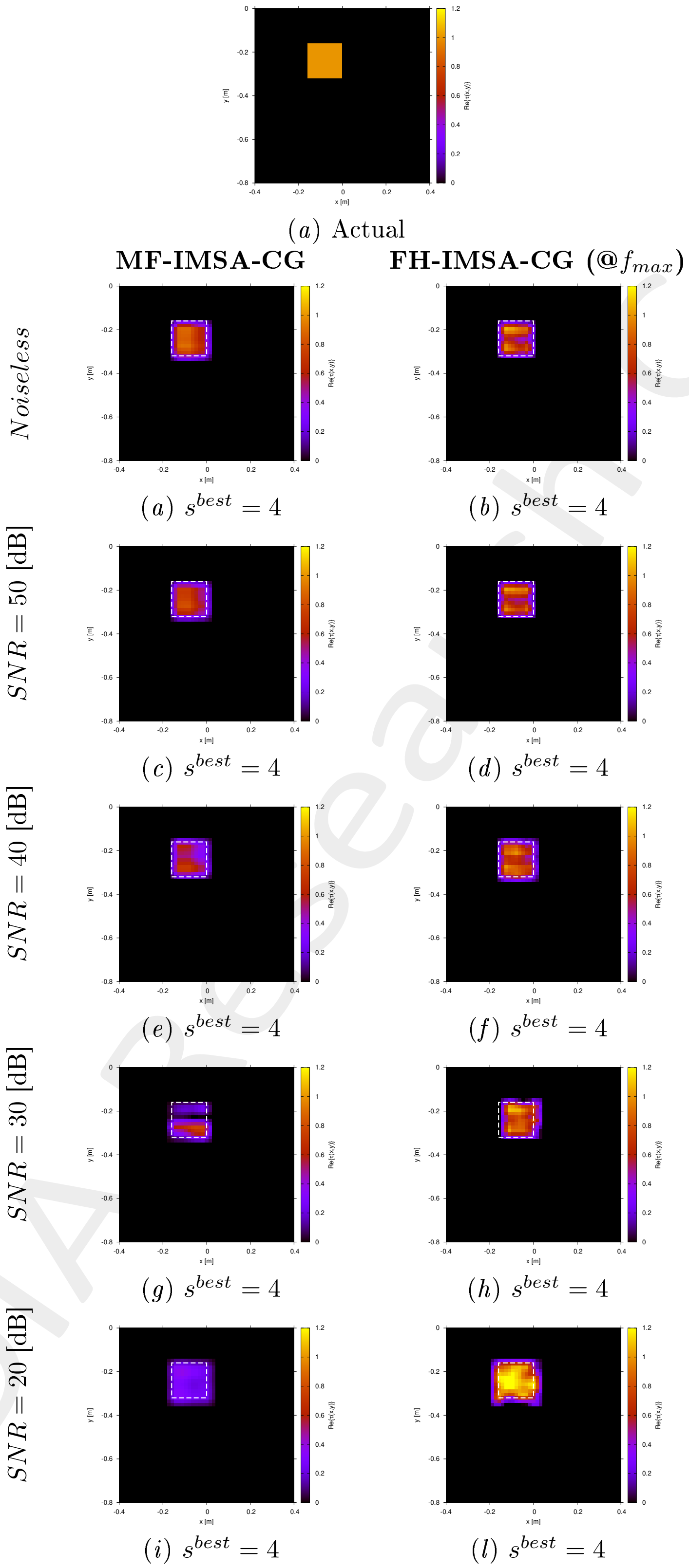


Figure 4: $MF-IMSA-CG$ vs. $FH-IMSA-CG$: Retrieved dielectric profiles at the $IMSA$ convergence step ($s^{best}$).

**Reconstruction Error** (@ $f_{max} = 600$ [MHz])

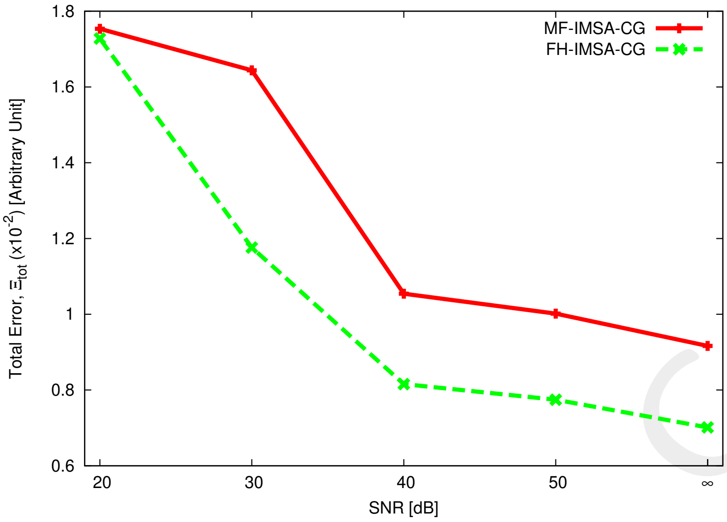


Figure 5: $MF-IMSA-CG$ vs. $FH-IMSA-CG$: Total reconstruction error vs. $SNR$.

## 2.2 Circular void ($\varepsilon_{r,obj} = 1.0$, $\sigma_{obj} = 0.0$ [S/m])

### 2.2.1 Parameters

**Background**

Inhomogeneous and nonmagnetic background composed by two half spaces

- Upper half space ($y > 0$ - air): $\varepsilon_{ra} = 1.0$, $\sigma_a = 0.0$;
- Lower half space ($y < 0$ - soil): $\varepsilon_{rb} = 4.0$, $\sigma_b = 10^{-3}$[S/m];

**Investigation domain** ($D_{inv}$)

- Side: $L_{D_{inv}} = 0.8$ [m];
- Barycenter: $\left(x_{bar}^{D_{inv}}, y_{bar}^{D_{inv}}\right) = (0.00, -0.4)$ [m];

**Time-Domain forward solver** ($FDTD$ - $GPRMax2D$)

- Side of the simulated domain: $L = 6$ [m];
- Number of cells: $N^{FDTD} = 750 \times 750 = 5.625 \times 10^5$;
- Side of the $FDTD$ cells $l^{FDTD} = 0.008$ [m];
- Simulation time window: $T^{FDTD} = 20 \times 10^{-9}$ [sec];
- Time step: $\Delta t^{FDTD} = 1.89 \times 10^{-11}$ [sec];
- Number of time samples: $N_t^{FDTD} = 1060$;
- Boundary conditions: perfectly matched layer ($PML$);
- Source type: Gaussian mono-cycle (first Gaussian pulse derivative, called "Ricker" in $GPRMax2D$)
  - Central frequency: $f_0 = 300$ [MHz];
  - Source amplitude: $A = 1.0$ [A];

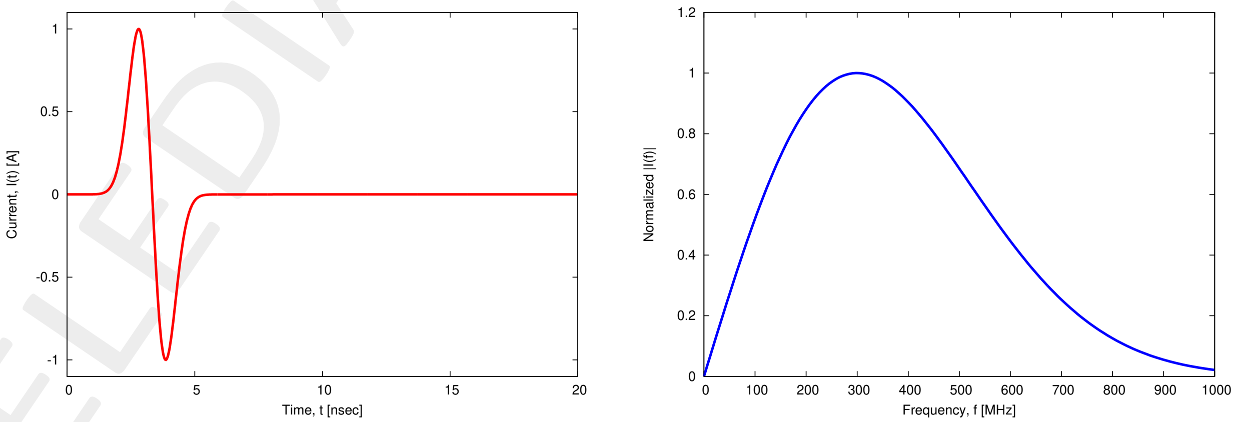


$(a)$ $(b)$

Figure 6: $GPRMax2D$ excitation signal. $(a)$ Time pulse, $(b)$ normalized frequency spectrum.

**Frequency parameters**

- Frequency range: $f \in [f_{min}, f_{max}] = [200.0, 600.0]$ [MHz] [?] ($-3$ [dB] bandwidth of the Gaussian Monocycle excitation centered at $f_0 = 300$ [MHz]);
- Frequency step: $\Delta f = 100$ [MHz] ($F = 5$ frequency steps in $[f_{min}, f_{max}]$);

| $f$ [MHz] | $\lambda_a$ [m] | $\lambda_b$ [m] | $f^*$ [MHz] |
|---|---|---|---|
| 200.0 | 1.50 | 0.75 | 200.5 |
| 300.0 | 1.00 | 0.50 | 297.6 |
| 400.0 | 0.75 | 0.37 | 401.1 |
| 500.0 | 0.60 | 0.30 | 498.1 |
| 600.0 | 0.50 | 0.25 | 601.6 |

Table 3: Considered frequencies and corresponding wavelength in the upper medium ($\lambda_a$, free space) and in the lower medium ($\lambda_b$, soil). $f^*$ is the nearest frequency sample available from transformed time-domain data, and represents the real frequency considered by the inversion algorithm.

**Scatterer**

- Type: Circular void;
- Barycenter: $(x_{obj}, y_{obj}) = (-0.16, -0.4)$ [m];
- Radius: $r_{obj} = 0.08$ [m];
- Electromagnetic properties: $\varepsilon_{r,obj} = 1.0$, $\sigma_{obj} = 0.0$ [S/m];
- Contrast function: $\tau = -3.0 + j0.03$ (@$f_{max} = 600$ [MHz]);

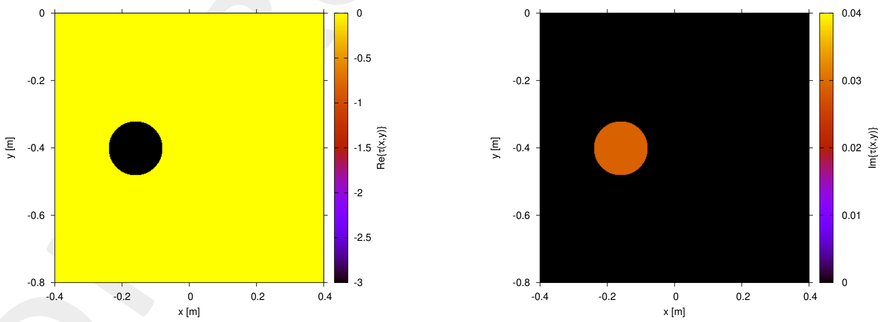


$(a)$ $(b)$

Figure 7: Actual object $(a)$ real part and $(b)$ imaginary part @$f_{max} = 600$ [MHz].

**Measurement setup**

- Considered frequency: $f_{min} = 200$ [MHz], $\lambda_b = 0.75$ [m].
- $\#DoFs = 2ka = \frac{2\pi}{\lambda_b} L\sqrt{2} = \frac{2\pi}{0.75} 0.8\sqrt{2} \simeq 9.5$;
- Number of views (sources): $V = 10$;

- $\min\{x_v\} = -0.5$ [m], $\max\{x_v\} = 0.5$ [m];
- height: $y_v = 0.1$ [m], $\forall v = 1, \dots, V$;

- Number of measurement points: $M = 9$;
  - $\min\{x_m\} = -0.5$ [m], $\max\{x_m\} = 0.5$ [m];
  - height: $y_m = 0.1$ [m], $\forall m = 1, \dots, M$;

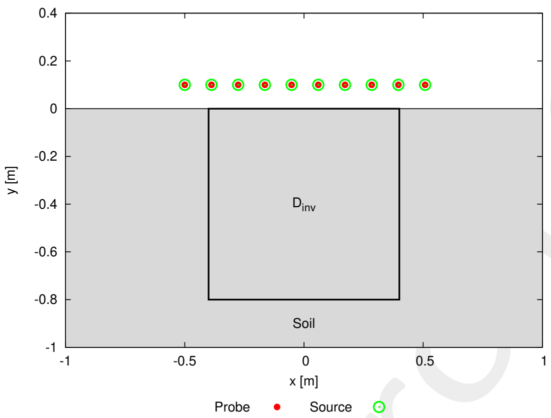


Figure 8: Location of the measurement points ($M = 9$) and of the sources ($V = 10$). Only one source is active for each view.

**Inverse solver parameters**

- **Shared parameters**
  - Weight of the state term of the functional: 1.0;
  - Weight of the data term of the functional: 1.0;
  - Convergence threshold: $10^{-10}$;
  - Variable ranges:
    * $\varepsilon_r \in [1.0, 4.0]$, $\sigma \in \left[0.0, 1.0 \times 10^{-3}\right]$ [S/m];
    * $\Re\left\{E_{tot}^{int}\right\} \in [-8, 8]$, $\Im\left\{E_{tot}^{int}\right\} \in [-8, 8]$;
  - Degrees of freedom:
    * Considered frequency: $f_{min} = 200$ [MHz], $\lambda_b = 0.75$ [m];
    * $\frac{(2ka)^2}{2} = \frac{\left(2\times\frac{2\pi}{\lambda_b}\times\frac{L\sqrt{2}}{2}\right)^2}{2} = 4\pi^2\left(\frac{L}{\lambda_b}\right)^2 = 4\pi^2\left(\frac{0.8}{0.75}\right)^2 \simeq 44.87$;
  - Number of cells: $N = 49 = 7 \times 7$;
  - Maximum number of $IMSA$ steps: $S = 4$;
  - Side ratio threshold: $\eta_{th} = 0.2$;

- $MF-IMSA-CG$ **parameters**

  - Maximum number of iterations: $I = 200$;

- $FH - IMSA - CG$ **parameters**

  - Maximum number of iterations: $I = 400$;

**Signal to noise ratio (on $E_{tot}(t)$)**

- $SNR = \{50, 40\}$ [dB] + Noiseless data.

| SNR on $E_{tot}(t)$ [dB] | Av. SNR on $E_{scatt}(f)$ [dB] |
|---|---|
| 50 | 45 |
| 40 | 35 |

Table 4: Average $SNR$ measured on the scattered field in frequency domain.

### 2.2.2 Results

**Final reconstructions (@$f_{max} = 600$ [MHz])**

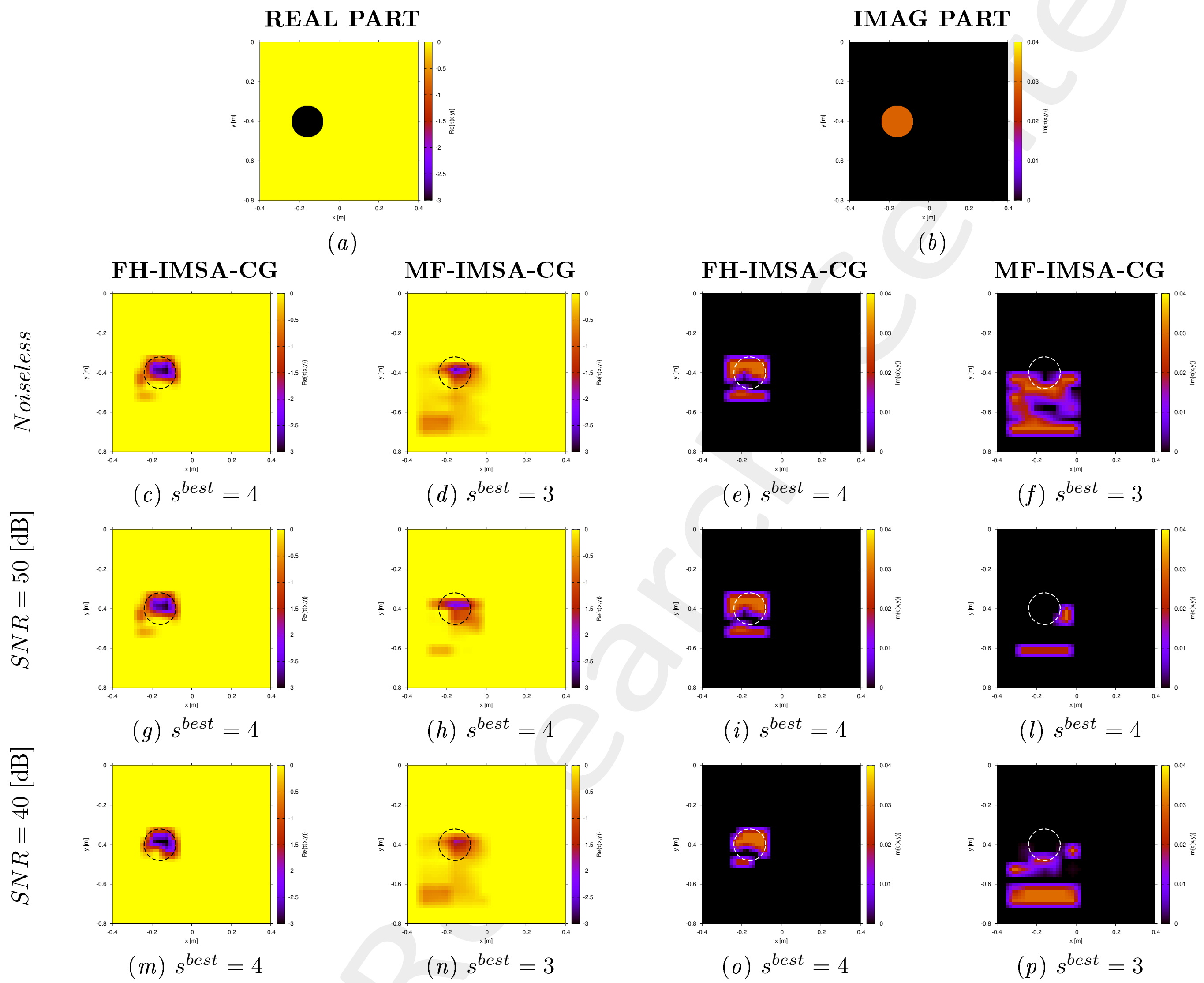


Figure 9: $MF-IMSA-PSO$ vs. $MF-IMSA-CG$: Retrieved dielectric profiles at the $IMSA$ convergence step ($s^{best}$).

## 2.3 Two-Square object ($\varepsilon_{r,obj} = 5.0$, $\sigma_{obj} = 10^{-3}$ [S/m])

### 2.3.1 Parameters

**Background**

Inhomogeneous and nonmagnetic background composed by two half spaces

- Upper half space ($y > 0$ - air): $\varepsilon_{ra} = 1.0$, $\sigma_a = 0.0$;
- Lower half space ($y < 0$ - soil): $\varepsilon_{rb} = 4.0$, $\sigma_b = 10^{-3}$[S/m];

**Investigation domain** ($D_{inv}$)

- Side: $L_{D_{inv}} = 0.8$ [m];
- Barycenter: $\left(x_{bar}^{D_{inv}}, y_{bar}^{D_{inv}}\right) = (0.00, -0.4)$ [m];

**Time-Domain forward solver** (*FDTD - GPRMax2D*)

- Side of the simulated domain: $L = 6$ [m];
- Number of cells: $N^{FDTD} = 750 \times 750 = 5.625 \times 10^5$;
- Side of the *FDTD* cells $l^{FDTD} = 0.008$ [m];
- Simulation time window: $T^{FDTD} = 20 \times 10^{-9}$ [sec];
- Time step: $\Delta t^{FDTD} = 1.89 \times 10^{-11}$ [sec];
- Number of time samples: $N_t^{FDTD} = 1060$;
- Boundary conditions: perfectly matched layer (*PML*);
- Source type: Gaussian mono-cycle (first Gaussian pulse derivative, called "Ricker" in *GPRMax2D*)
  - Central frequency: $f_0 = 300$ [MHz];
  - Source amplitude: $A = 1.0$ [A];

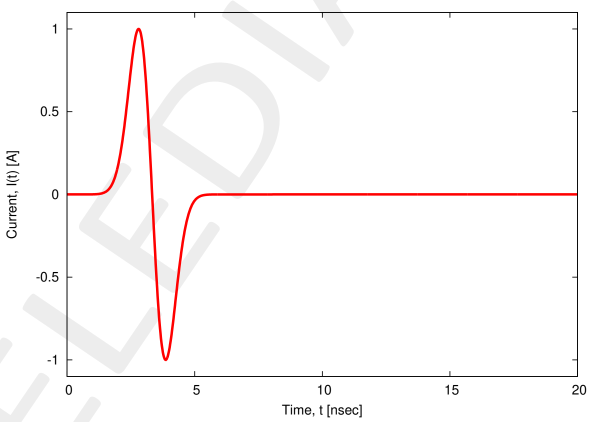

(*a*)

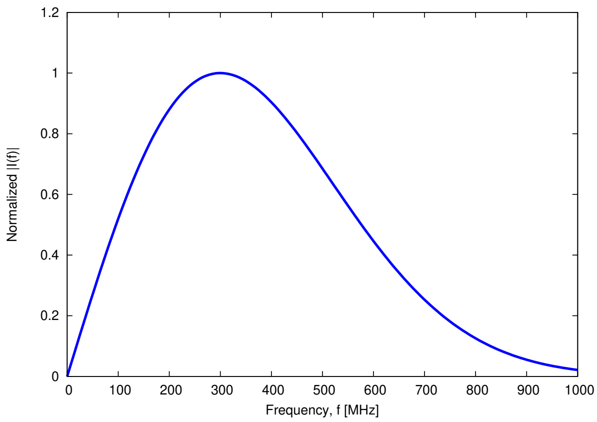

(*b*)

Figure 10: *GPRMax2D* excitation signal. (*a*) Time pulse, (*b*) normalized frequency spectrum.

**Frequency parameters**

- Frequency range: $f \in [f_{min}, f_{max}] = [200.0, 600.0]$ [MHz] [?] ($-3$ [dB] bandwidth of the Gaussian Monocycle excitation centered at $f_0 = 300$ [MHz]);
- Frequency step: $\Delta f = 100$ [MHz] ($F = 5$ frequency steps in $[f_{min}, f_{max}]$);

| $f$ [MHz] | $\lambda_a$ [m] | $\lambda_b$ [m] | $f^*$ [MHz] |
|---|---|---|---|
| 200.0 | 1.50 | 0.75 | 200.5 |
| 300.0 | 1.00 | 0.50 | 297.6 |
| 400.0 | 0.75 | 0.37 | 401.1 |
| 500.0 | 0.60 | 0.30 | 498.1 |
| 600.0 | 0.50 | 0.25 | 601.6 |

Table 5: Considered frequencies and corresponding wavelength in the upper medium ($\lambda_a$, free space) and in the lower medium ($\lambda_b$, soil). $f^*$ is the nearest frequency sample available from transformed time-domain data, and represents the real frequency considered by the inversion algorithm.

**Scatterer**

- Type: Two squares;
- Electromagnetic properties: $\varepsilon_{r,obj} = 5.0$, $\sigma_{obj} = 10^{-3}$ [S/m] ($\sigma_{obj} = \sigma_b$);
- Contrast function: $\tau = 1.0 + j0.0$

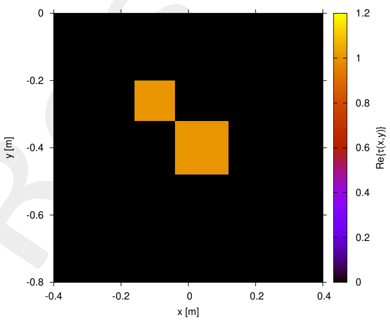


Figure 11: Actual object ($\tau = 1.0$).

**Measurement setup**

- Considered frequency: $f_{min} = 200$ [MHz], $\lambda_b = 0.75$ [m].
- $\#DoFs = 2ka = \frac{2\pi}{\lambda_b} L\sqrt{2} = \frac{2\pi}{0.75} 0.8\sqrt{2} \simeq 9.5$;
- Number of views (sources): $V = 10$;
  - $\min\{x_v\} = -0.5$ [m], $\max\{x_v\} = 0.5$ [m];
  - height: $y_v = 0.1$ [m], $\forall v = 1, \dots, V$;
- Number of measurement points: $M = 9$;

- $\min\{x_m\} = -0.5$ [m], $\max\{x_m\} = 0.5$ [m];
- height: $y_m = 0.1$ [m], $\forall m = 1, \dots, M$;

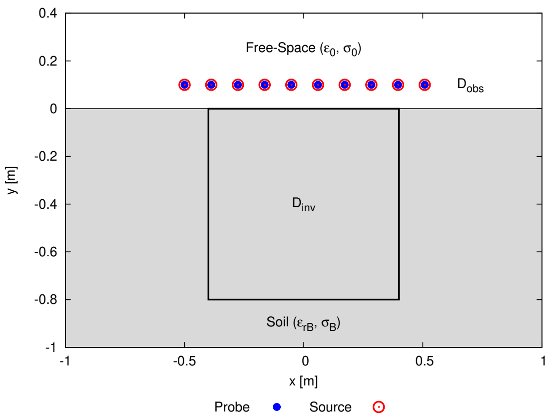


Figure 12: Location of the measurement points ($M = 9$) and of the sources ($V = 10$). Only one source is active for each view.

**Inverse solver parameters**

- **Shared parameters**
  - Weight of the state term of the functional: 1.0;
  - Weight of the data term of the functional: 1.0;
  - Convergence threshold: $10^{-10}$;
  - Variable ranges:
    - $\varepsilon_r \in [4.0, 5.2]$, $\sigma \in \left[8.0 \times 10^{-4}, 1.2 \times 10^{-3}\right]$ [S/m];
    - $\Re\left\{E_{tot}^{int}\right\} \in [-8, 8]$, $\Im\left\{E_{tot}^{int}\right\} \in [-8, 8]$;
  - Degrees of freedom:
    - Considered frequency: $f_{min} = 200$ [MHz], $\lambda_b = 0.75$ [m];
    - $\frac{(2ka)^2}{2} = \frac{\left(2\times\frac{2\pi}{\lambda_b}\times\frac{L\sqrt{2}}{2}\right)^2}{2} = 4\pi^2\left(\frac{L}{\lambda_b}\right)^2 = 4\pi^2\left(\frac{0.8}{0.75}\right)^2 \simeq 44.87$;
  - Number of cells: $N = 49 = 7 \times 7$;
  - Maximum number of $IMSA$ steps: $S = 4$;
  - Side ratio threshold: $\eta_{th} = 0.2$;
- $MF - IMSA - CG$ **parameters**
  - Maximum number of iterations: $I = 200$;
- $FH - IMSA - CG$ **parameters**
  - Maximum number of iterations: $I = 400$;

**Signal to noise ratio (on $E_{tot}\left(t\right)$)**

- $SNR = \{50, 40\}$ [dB] + Noiseless data.

| SNR on $E_{tot}\left(t\right)$ [dB] | Av. SNR on $E_{scatt}\left(f\right)$ [dB] |
|---|---|
| 50 | 36 |
| 40 | 26 |

Table 6: Average $SNR$ measured on the scattered field in frequency domain.

### 2.3.2 Results

**Final reconstructions (@$f_{max} = 600$ [MHz])**

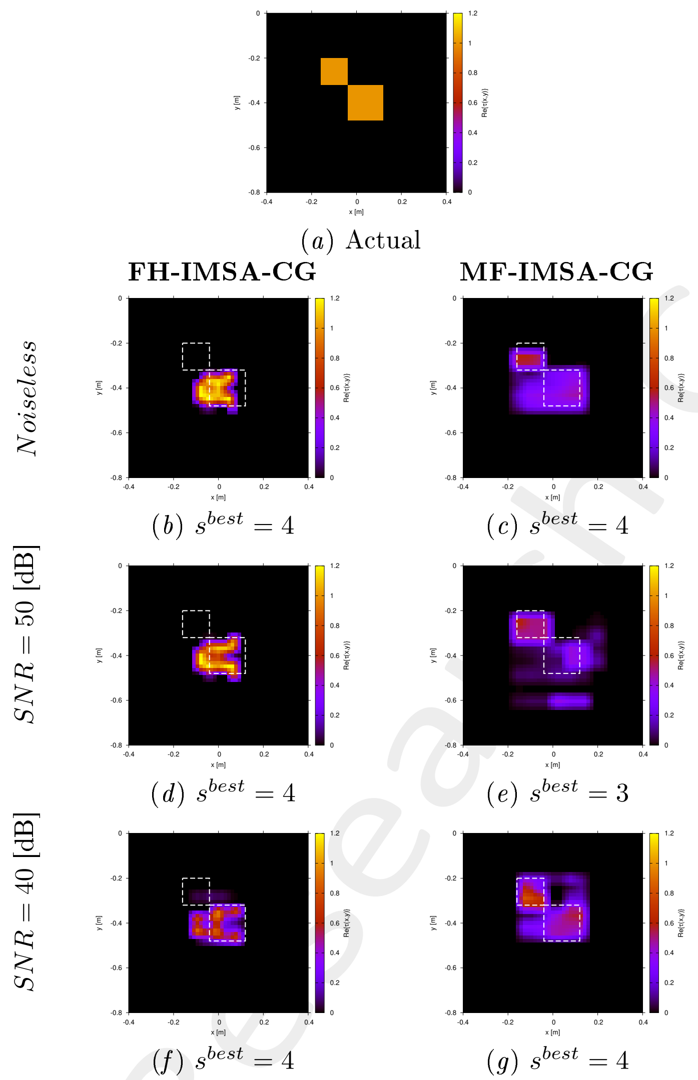


Figure 13: $FH-IMSA-CG$ vs. $MF-IMSA-CG$: Retrieved dielectric profiles at the $IMSA$ convergence step ($s^{best}$) @$f_{max} = 600$ [MHz].

**More information on the topics of this document can be found in the following list of references.**

# References


[1] P. Rocca, M. Benedetti, M. Donelli, D. Franceschini, and A. Massa, “Evolutionary optimization as applied to inverse scattering problems,” *Inverse Probl.*, vol. 25, no. 12, pp. 1-41, 2009 (DOI: 10.1088/0266-5611/25/12/123003).

[2] P. Rocca, G. Oliveri, and A. Massa, “Differential Evolution as applied to electromagnetics,” *IEEE Antennas Propag. Mag.*, vol. 53, no. 1, pp. 38-49, Feb. 2011 (DOI: 10.1109/MAP.2011.5773566).

[3] M. Salucci, G. Oliveri, and A. Massa, “GPR prospecting through an inverse scattering frequency-hopping multi-focusing approach,” *IEEE Trans. Geosci. Remote Sens.*, vol. 53, no. 12, pp. 6573-6592, Dec. 2015 (DOI: 10.1109/TGRS.2015.2444391).

[4] M. Salucci, L. Poli, N. Anselmi and A. Massa, “Multifrequency particle swarm optimization for enhanced multiresolution GPR microwave imaging,” *IEEE Trans. Geosci. Remote Sens.*, vol. 55, no. 3, pp. 1305-1317, Mar. 2017 (DOI: 10.1109/TGRS.2016.2622061).

[5] A. Massa, P. Rocca, and G. Oliveri, “Compressive sensing in electromagnetics - A review,” *IEEE Antennas Propag. Mag.*, pp. 224-238, vol. 57, no. 1, Feb. 2015 (DOI: 10.1109/MAP.2015.2397092).

[6] A. Massa and F. Texeira, “Guest-Editorial: Special Cluster on Compressive Sensing as Applied to Electromagnetics,” *IEEE Antennas Wireless Propag. Lett.*, vol. 14, pp. 1022-1026, 2015 (DOI: 10.1109/LAWP.2015.2425011).

[7] N. Anselmi, G. Oliveri, M. Salucci, and A. Massa, “Wavelet-based compressive imaging of sparse targets,” *IEEE Trans. Antennas Propag.*, vol. 63, no. 11, pp. 4889-4900, Nov. 2015 (DOI: 10.1109/TAP.2015.2444423).

[8] G. Oliveri, N. Anselmi, and A. Massa, “Compressive sensing imaging of non-sparse 2D scatterers by a total-variation approach within the Born approximation,” *IEEE Trans. Antennas Propag.*, vol. 62, no. 10, pp. 5157-5170, Oct. 2014 (DOI: 10.1109/TAP.2014.2344673).

[9] T. Moriyama, G. Oliveri, M. Salucci, and T. Takenaka, “A multi-scaling forward-backward time-stepping method for microwave imaging,” *IEICE Electron. Expr.*, vol. 11, no. 16, pp. 1-12, Aug. 2014 (DOI: 10.1587/elex.11.20140578).

[10] T. Moriyama, M. Salucci, M. Tanaka, and T. Takenaka, “Image reconstruction from total electric field data with no information on the incident field,” *J. Electromagnet. Wave.*, vol. 30, no. 9, pp. 1162-1170, 2016 (DOI: 10.1080/09205071.2016.1182876).

[11] F. Viani, L. Poli, G. Oliveri, F. Robol, and A. Massa, “Sparse scatterers imaging through approximated multi-task compressive sensing strategies,” *Microw. Opt. Technol. Lett.*, vol. 55, no. 7, pp. 1553-1557, Jul. 2013 (DOI: 10.1002/mop.27612).

[12] M. Salucci, L. Poli, and A. Massa, “Advanced multi-frequency GPR data processing for non-linear deterministic imaging,” *Signal Processing - Special Issue on 'Advanced Ground-Penetrating Radar Signal-Processing Techniques*,' vol. 132, pp. 306-318, Mar. 2017 (DOI: 10.1016/j.sigpro.2016.06.019).

[13] M. Salucci, N. Anselmi, G. Oliveri, P. Calmon, R. Miorelli, C. Reboud, and A. Massa, “Real-time NDT-NDE through an innovative adaptive partial least squares SVR inversion approach,” *IEEE Trans. Geosci. Remote Sens.*, vol. 54, no. 11, pp. 6818-6832, Nov. 2016 (DOI: 10.1109/TGRS.2016.2591439).

[14] L. Poli, G. Oliveri, and A. Massa, “Imaging sparse metallic cylinders through a local shape function bayesian compressing sensing approach,” *J. Opt. Soc. Am. A*, vol. 30, no. 6, pp. 1261-1272, Jun. 2013 (DOI: 10.1364/JOSAA.30.001261).